The Posterior Location of the Dilator Muscle Induces Anterior Iris Bowing during Dilation, Even in the Absence of Pupillary Block

Rouzbeh Amini,[1,2] *Julie E. Whitcomb,*[3] *Muhammad K. Al-Qaisi,*[1] *Taner Akkin,*[1] *Sara Jouzdani,*[3] *Syril Dorairaj,*[4] *Tiago Prata,*[4] *Elena Illitchev,*[5] *Jeffrey M. Liebmann,*[4,5] *Robert Ritch,*[4,6] *and Victor H. Barocas*[1]

Purpose. To examine the effect of the posterior location of the dilator on iris anterior curvature during dilation.

Methods. An in vivo human study, an ex vivo porcine experiment, and an in silico computational model were performed in parallel. Iris anterior curvature was measured in vivo before and after dilation by time-domain slit lamp optical coherence tomography (SL-OCT). All patients ($n = 7$) had undergone laser peripheral iridotomy to eliminate any pupillary block due to primary angle-closure glaucoma. In the ex vivo experiments, isolated porcine irides ($n = 30$) were secured at the periphery and immersed in an oxygenated Krebs-Ringer buffer. Dilation was induced pharmaceutically by the addition of 2.5% phenylephrine and 1% tropicamide. An in-house optical coherence tomography (OCT) system was used to obtain iris images before and after dilation. A finite element model was also developed based on typical geometry of the iris from the initial OCT image. The iris was modeled as a neo-Hookean solid, and the active muscle component was applied only to the region specified as the dilator.

Results. An increase in curvature and a decrease in chord length after dilation were observed in both experiments. In both the in vivo and ex vivo experiments, the curvature-to-chord length ratio increased significantly during dilation. Computer simulations agreed well with the experimental results only when the proper anatomic position of dilator was used.

Conclusions. The posterior location of the dilator contributes to the anterior iris bowing via a nonpupillary block dependent mechanism. (*Invest Ophthalmol Vis Sci.* 2012;53:1188–1194) DOI:10.1167/iovs.11-8408

Anterior bowing of the iris, resulting in a narrow or closed angle, is often attributed to pupillary block,[1–3] even though it is recognized that the angle can close by multiple mechanisms, some independent of pupillary block. In particular, the mechanism by which the iris bows anteriorly during dilation[4] is unclear. We have shown theoretically[5] that the pressure increase from blocking the steady flow of aqueous cannot explain the increased anterior bowing when the pupil dilates, and Woo et al.[4] reported that the anterior bowing during dilation occurs within seconds, far too quickly for aqueous humor to build up in the posterior chamber. Yamamoto et al.[6] reported that when pupils in rabbits with a laser peripheral iridotomy (LPI) were dilated, the aqueous flowed posteriorly, not anteriorly, which implies that the anterior chamber pressure was, in fact, higher. In some cases, LPI does not lead to opening of the angle, and after dilation, the angle can still narrow and the iris can still bow forward considerably.[7–9] Taken together, these observations require that non–pupillary-block mechanisms for anterior iris bowing, especially during dilation, be considered. In this study, we explored the hypothesis that the anatomy of the iris, specifically the posterior position of the dilator muscle within the iris, contributes to the spontaneous anterior curvature of the iris during dilation, independent of pupillary block.

Methods

This work included three parallel studies:

- In vivo experiments, in which the curvature of the iris was measured before and after dilation in a set of subjects, all of whom had undergone LPIs, eliminating any pupillary block.
- Ex vivo experiments, in which the isolated porcine iris was dilated pharmacologically and imaged via optical coherence tomography (OCT), to determine the iris contour.
- In silico computer simulations, in which realistic geometry and dilator placement were used to model the ex vivo experiments.

In Vivo Experiments

All patients had been diagnosed previously with anatomically narrow-angles (ANAs) and primary angle-closure glaucoma (PACG). Patients diagnosed with ANAs who underwent LPI surgery to open the angle were imaged by slit lamp optical coherence tomography (SL-OCT) in light and dark conditions. Institutional review board approval was obtained, as was written informed consent for all subjects. At the time of imaging, all subjects' angles were noted to be open. The SL-OCT system (Heidelberg Engineering, GmbH, Dossenheim, Germany) had an optical axial image resolution <25 μm and a lateral resolution of 20

From the Departments of [1]Biomedical Engineering and [3]Mechanical Engineering, University of Minnesota, Minneapolis, Minnesota; the [2]Department of Bioengineering, University of Pittsburgh, Pittsburgh, Pennsylvania; the [4]Einhorn Clinical Research Center, New York Eye and Ear Infirmary, New York, New York; the [5]New York University School of Medicine, New York, New York; and the [6]Department of Ophthalmology, New York Medical College, Valhalla, New York.

Supported by National Institutes of Health Grant EY 15795 and the Ira and Judith Robinson Research Fund of the New York Glaucoma Research Institute, New York, NY. Computations were facilitated by a supercomputing resources grant from the University of Minnesota Supercomputing Institute for Digital Simulation and Advanced Computation.

Submitted for publication August 12, 2011; revised November 10, 2011; accepted January 16, 2012.

Disclosure: **R. Amini**, None; **J.E. Whitcomb**, None; **M.K. Al-Qaisi**, None; **T. Akkin**, None; **S. Jouzdani**, None; **S. Dorairaj**, None; **T. Prata**, None; **E. Illitchev**, None; **J.M. Liebmann**, None; **R. Ritch**, None; **V.H. Barocas**, None

Corresponding author: Victor H. Barocas, Department of Biomedical Engineering, University of Minnesota, 7-105 Hasselmo Hall, 312 Church Street, SE, Minneapolis, MN 55455; baroc001@umn.edu.

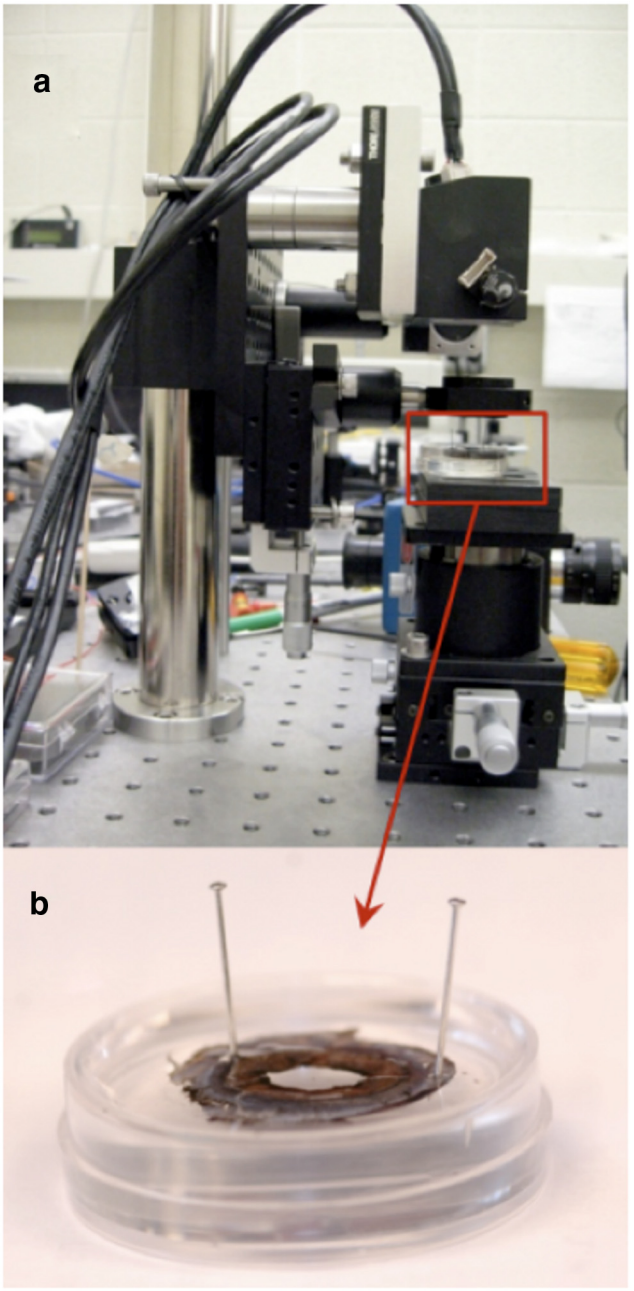

FIGURE 1. Ex vivo experimental setup. Experimental setup of the in-house (**a**) OCT imaging system with the (**b**) iris sample pinned in the Petri dish.

to 100 μm. Initially, five high-quality cross-sectional images were taken in each subject while the subject was in the sitting position in the dark. Subsequently, images were acquired under standardized lighting conditions (300 lux), using a 5 × 1-mm light beam set at the maximum intensity of the device. Subjects were instructed to blink normally and to fixate with the nonimaged eye on a target 1 m from the device to minimize accommodation artifact. All images were taken horizontally through the center of the pupil to avoid interference with the lid margins, and iris crypts were avoided whenever possible. Quality-control parameters were defined as a well-centered image, a clearly defined scleral spur, and the absence of artifacts. Patients with as diagnosis of exfoliation syndrome, uveitis, or pigmentary glaucoma, were excluded, as were those with previous intraocular surgery. Patients who were on systemic α-1 adrenergic receptor antagonists (such as Flomax; tamsulosin hydrochloride; Boehringer-Ingelheim Pharmaceuticals, GmbH., Ingelheim am Rhein, Germany) or on topical medications known to alter the iris configuration[10,11] were also excluded. Whenever both eyes were eligible, one eye was randomly selected. The study was conducted in accordance with the ethical standards stated in the 1964 Declaration of Helsinki and was approved by the institutional review board (IRB).

Images were analyzed with ImageJ software (developed by Wayne Rasband, National Institutes of Health, Bethesda, MD; available at http://rsb.info.nih.gov/ij/index.html).[12] Chord length,[4] iris curvature,[13] and iris concavity ratio[14] were calculated. Positive curvature indicates anterior bowing (concavity) whereas negative curvature reflects posterior bowing. The iris concavity ratio, as described previously, is defined as the ratio of iris curvature to chord length, which has the advantage of being a scale-invariant measure of curvature.[14] Results were compared by two-sided paired *t*-test assuming equal variance.

Ex Vivo Experiments

Experiments were performed on 30 isolated porcine irides and were in compliance with the ARVO Statement for Use of Animals in Ophthalmic and Vision Research. The irides were tested within 2 to 6 hours after death and prepared as described previously.[15] The isolated irides were pinned at two locations on the periphery of the tissue in a Petri dish with a silicone-based polymer lining (Fig. 1).

The irides were immersed at room temperature in a 5-mL bath of oxygenated Krebs-Ringer buffer to maintain a physiological pH of 7.4. Before dilation, reference images of the iris were taken via the fiber-based, swept-source OCT system[16] shown schematically in Figure 2.

The system operated in the Fourier domain, by which modulations on the optical spectrum were related to the spatial information along a depth profile called an A-line.[17] After the initial image was captured, the irides were dilated pharmaceutically by addition of 40 μL of 2.5% phenylephrine and 40 μL of 1% tropicamide solutions. Images of the dilated iris were taken every 40 seconds for 10 to 15 minutes. The initial and final images were analyzed using ImageJ[12] to calculate the change in pupil diameter, chord length (A–B), curvature (C–D), and the concavity ratio (C–D/A–B). These measurements are described in Figure 3a. Results were compared by two-sided paired *t*-test assuming equal variance.

In Silico Studies

A realistic finite-element mesh of the iris was constructed on the basis of initial OCT image of the nondilated iris (Fig. 3b). The dilator muscle is a very thin, radially aligned smooth muscle located on the posterior surface of the iris. The dilator extends centrally to the midpoint of the sphincter muscle. For humans, the average thickness of the dilator is 4.0 to 8.5 μm,[11,18] whereas in the porcine model the average dilator thickness is 26 μm.[19] We placed the dilator muscle in the posterior portion of the iris, on the basis of histologic analysis of the porcine iris (Fig. 4). The iris was modeled as a nearly incompressible neo-Hookean solid[20] governed by the static stress balance:

$$\nabla \cdot \boldsymbol{\sigma} = 0 \qquad (1)$$

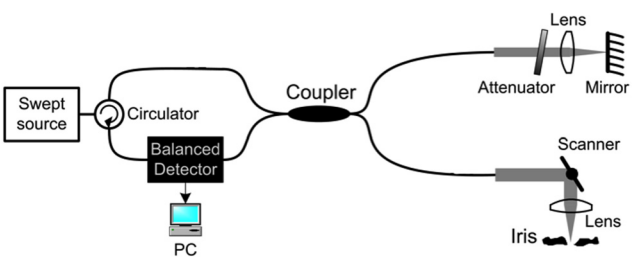

FIGURE 2. The OCT system used to image the iris during dilation.[16]

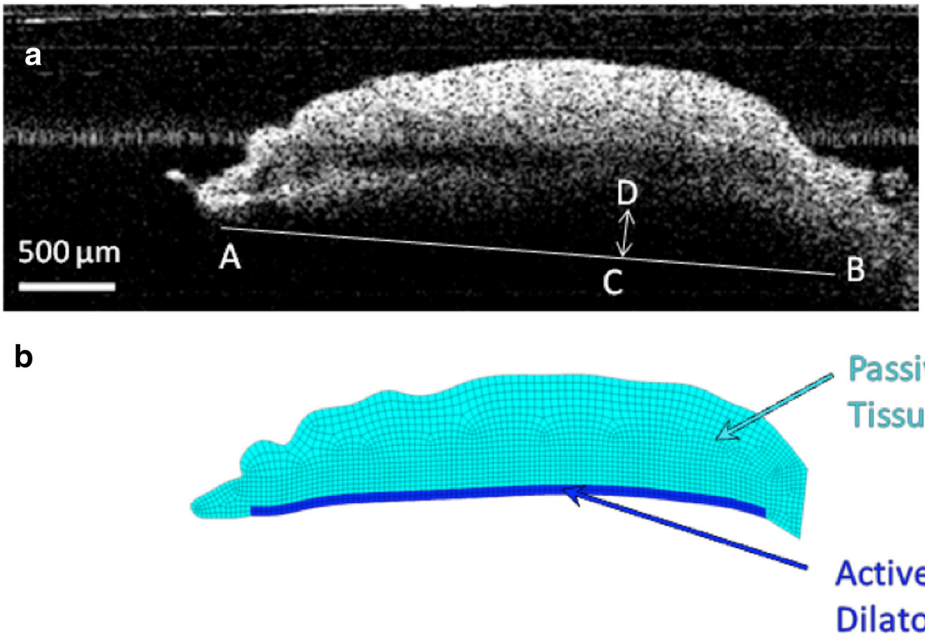

FIGURE 3. (**a**) OCT image of the iris before the dilator is activated. Iris chord length (A–B) is defined as the distance from the tip of the iris to the periphery; iris curvature (C–D) is defined as the longest distance between the iris chord and posterior epithelium. (**b**) Finite element model based on the OCT image of the iris before dilation. The region modeled as the active dilator muscle is marked with the darker color.

where $\boldsymbol{\sigma}$ was the Cauchy stress tensor, and derivatives of the stress were with respect to the current coordinate system. The Cauchy stress tensor was defined by neo-Hookean, $\boldsymbol{\sigma}_{NH}$, and active dilator, $\boldsymbol{\sigma}_{D}$, contributions:

$$\boldsymbol{\sigma} = \boldsymbol{\sigma}_{NH} + \boldsymbol{\sigma}_{D} \quad (2)$$

The neo-Hookean stress was defined by

$$\boldsymbol{\sigma}_{NH} = \frac{G}{\det \mathbf{F}}(\mathbf{B} - \mathbf{I}) + \frac{2G\nu}{(1-2\nu)\det \mathbf{F}}\ln(\det \mathbf{F})\mathbf{I} \quad (3)$$

where G was the shear modulus, ν the Poisson's ratio, **I** the identity tensor, **F** the deformation gradient, and **B** the left Cauchy-Green deformation tensors, in which **F** and **B** were defined as follows:

$$\mathbf{F} = \frac{d\mathbf{x}}{d\mathbf{X}} \quad (4)$$

$$\mathbf{B} = \mathbf{F}\mathbf{F}^{T} \quad (5)$$

with **x** being the current position of a material point and **X** being its resting position.

The iris shear modulus (G = 9 kPa) and Poisson's ratio (ν = 0.49) were based on our previous studies.[21] The dilator term $\boldsymbol{\sigma}_{D}$ was applied only in the dilator region (represented by the darker blue in Fig. 3b). To ensure that the muscle contraction was always in the direction of the nondeformed dilator muscle, it was defined by σ_{Act}, the scalar muscle contraction stress, and $\mathbf{e}_{s}$, the unit vector representing the direction of nondeformed dilator muscle:

$$\boldsymbol{\sigma}_{D} = \sigma_{Act}(\mathbf{F}\mathbf{e}_{s}) \otimes (\mathbf{F}\mathbf{e}_{s}) \quad (6)$$

The Galerkin finite-element method was employed for spatial discretization of the mathematical model. Mesh-generation software (GAMBIT; Fluent, Inc., Lebanon, NH) was used to generate the finite element mesh. The nonlinear algebraic equation system was solved using Newton-Raphson iteration and the direct solver MUMPS.[22]

The model was used to simulate spontaneous contraction of the dilator muscle ex vivo, based on the experiments described above. The pupil diameter was increased from 5.0 to 7.0 mm by applying a muscle-contraction stress σ_{Act}. To assess the importance of the location of the dilator muscle, three simulations were performed. In

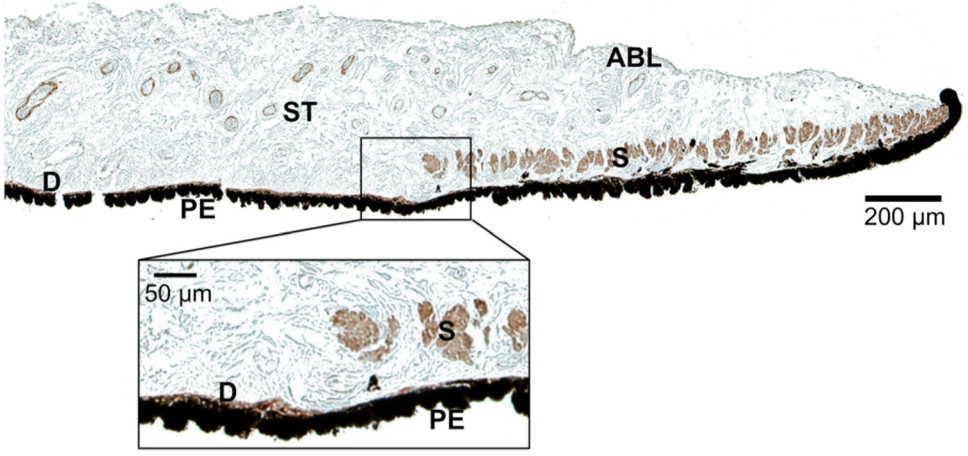

FIGURE 4. Histologic image of the pupillary and midperipheral portions of the porcine iris. Monoclonal anti-human α-smooth muscle actin stain was used to differentiate the muscular tissues, including the sphincter (S) and dilator (D). The pigment epithelium anterior border layer (ABL); stroma (ST), which is a loosely arranged collagen network; and another thick layer of pigment epithelial (PE) cells on the posterior surface of the iris is also identifiable. Magnification of the midperiphery regions illustrates that dilator muscle lies on the posterior iris surface and is very thin compared with the sphincter muscle.

TABLE 1. ANA Patient Information

Sex	Race	Age (y)	Diagnosis	Eye	Refractive Error		IOP (mmHg)	
					OD	OS	OD	OS
F	C	68	PACG	OS	+2.75	+2.50	15	15
M	C	66	PACG	OD	+2.50	+2.00	15	16
M	H	62	PACG	OD	−2.00	−1.50	15	17
F	C	50	ANA	OD	−7.75	−7.75	14	15
M	C	47	ANA	OU	+1.25	+1.50	14	14
M	C	58	PACG	OD	−0.75	−1.00	15	16
M	H	60	ANA	OD	+1.00	+0.75	19	19

All patients had had previous LPI surgeries on one (OD or OS) eye after receiving a diagnosis of PACG or ANA. Patients' sex and race (Caucasian C or Hispanic H) is noted. The refractive error in both eyes is given along with the IOP at the time of the SL-OCT.

the first case, the dilator muscle was located in the posterior iris as in the histologic porcine images. In the second case, the dilator layer was artificially positioned more anteriorly. Finally, in the third case, the entire thickness of the iris was modeled as the active dilator muscle. In all three cases, the iris chord length, and the iris curvature (Fig. 3a) were calculated from the model.

RESULTS

In Vivo Experiments

We examined seven patients with diagnosis of ANA and/or PACG; patient details are given in Table 1. The measurements for the patients are shown in Figure 5. The pupil diameter (Fig. 5a) was 2.73 ± 0.39 mm in the light and increased to 4.71 ± 0.55 mm ($P < 0.001$) in the dark (mean ± 95% CI, $n = 7$). The iris chord length (Fig. 5b) decreased significantly from 5.18 ± 0.35 to 4.23 ± 0.37 mm ($P < 0.0001$). Both the curvature and concavity ratio increased, but only the concavity ratio increased significantly. The curvature (Fig. 5c) increased from 0.13 ± 0.09 to 0.16 ± 0.02 mm ($P = 0.481$) and the concavity ratio (Fig. 5d) from 0.026 ± 0.01 to 0.04 ± 0.01 mm ($P = 0.004$), including a significant change in shape due to the combination of chord length and curvature changes.

Ex Vivo Experiments

Figure 6 shows a pinned porcine iris before (Fig. 6a) and after (Fig. 6b) dilation. The pupil diameter increased in the experiment, indicating that there was still activation of the dilator muscle (phenylephrine) and possibly relaxation of the sphincter muscle (tropicamide). The bar graph in Figure 7a shows that the pupil diameter increased from 2.82 ± 0.16 to 3.72 ± 0.21 mm (mean ± 95% CI, $n = 30$; $P < 0.001$) after the addition of the 40 μL of 2.5% phenylephrine and 40 μL of 1% tropicamide. The iris chord length (Fig. 7b) decreased from 1.43 ± 0.11 to 1.12 ± 0.09 mm ($P < 0.0001$) after activation of the dilator muscle. The iris curvature also changed after dilation (Fig. 7c), increasing from 0.12 ± 0.01

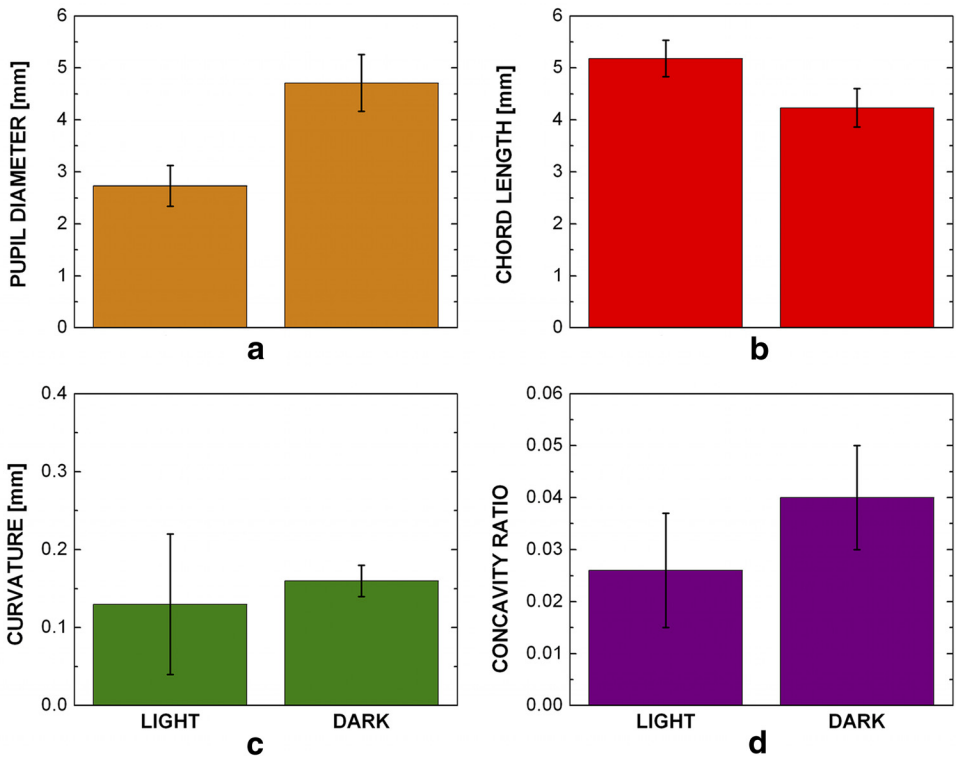

FIGURE 5. In vivo ANA patients' iris chord length, curvature, and concavity ratio results. (**a**) The pupil diameter increased ($P < 0.0001$), (**b**) the iris chord length decreased ($P < 0.0001$), (**c**) the iris curvature increased ($P = 0.481$), and (**d**) the concavity ratio increased ($P = 0.004$) after dilation in the dark (bars, 95% confidence interval; $n = 7$).

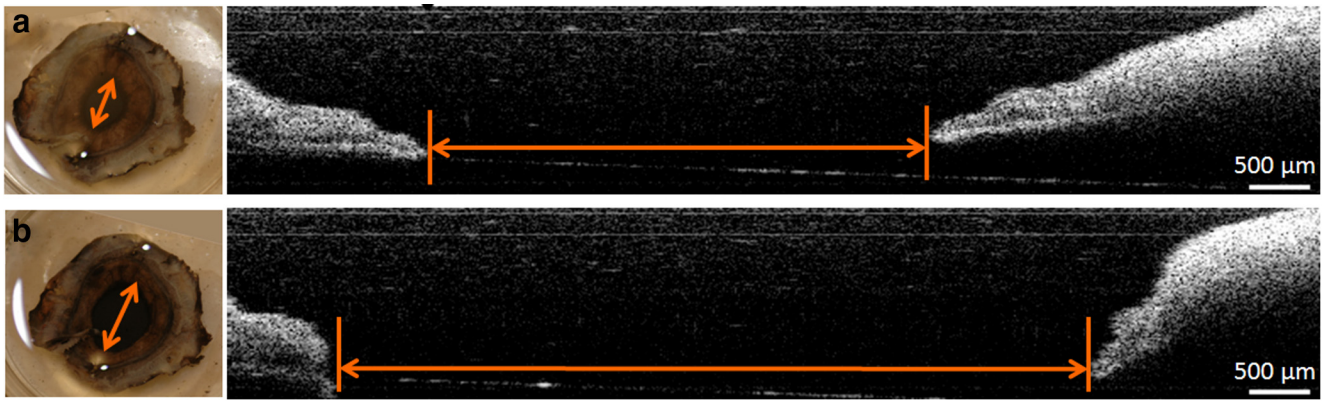

FIGURE 6. Ex vivo pupil dilation results. Images taken before (**a**) and after (**b**) the addition of 40 µL of 2.5% phenylephrine and 40 µL of 1% tropicamide to the bath solution. On the left is a top-down view of an iris with the anterior surface facing up using a digital camera and in the middle is the cross section of the iris detected by the OCT imaging system. The pupil diameter (*arrows*) is shown to visibly increase after the addition of the drugs.

to 0.20 ± 0.02 mm ($P < 0.002$). The concavity ratio also changed significantly (Fig. 7d), increasing from 0.09 ± 0.01 to 0.21 ± 0.02 ($P < 0.0001$) after drug-induced dilation. These results were all consistent with the in vivo experiments.

In Silico Studies

Figure 8 shows the iris deformation after dilation in a typical ex vivo experiment compared with the three simulation results created based on the undeformed geometry the tissue. In both the experiment (Fig. 8a) and the realistic model, in which the dilator muscle was positioned in the posterior portion of the iris (Fig. 8b), the iris curvature increased and the iris chord length decreased. The unrealistic models, however, did not predict the experimental results correctly. Positioning the dilator anteriorly within the iris led to a smaller increase in the iris curvature after dilation (Fig. 8c). Modeling the whole thickness of iris as the active muscle led to a decrease in the iris curvature (i.e., shift to the posterior). As quantified in Figure 9, the realistic model was the only one that predicted the iris concavity ratio after dilation consistent with the experimental results.

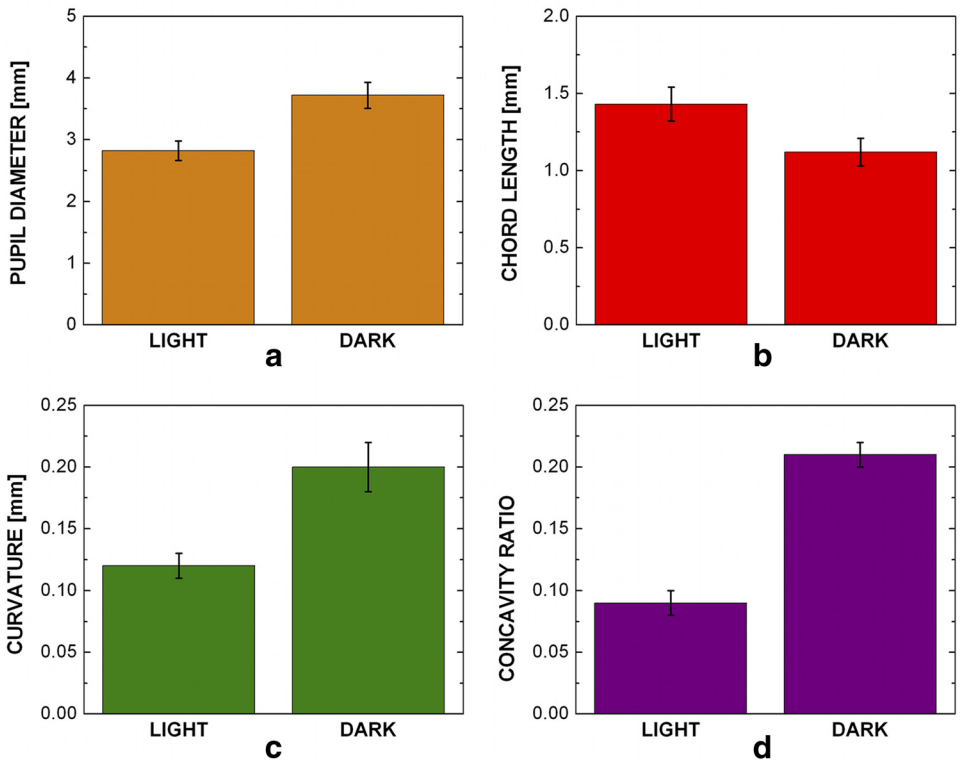

FIGURE 7. Ex vivo iris pupil diameter, chord length, curvature, and concavity ratio results. All measurements showed a significant difference before and after the addition of the dilation drugs. The pupil diameter (**a**) increased significantly ($P < 0.001$) after the addition of the drugs, the chord length (**b**) decreased ($P < 0.0001$), the curvature (**c**) increased ($P < 0.002$), and the (**d**) concavity ratio ($P < 0.0001$) increased (bars, 95% confidence interval, $n = 30$).

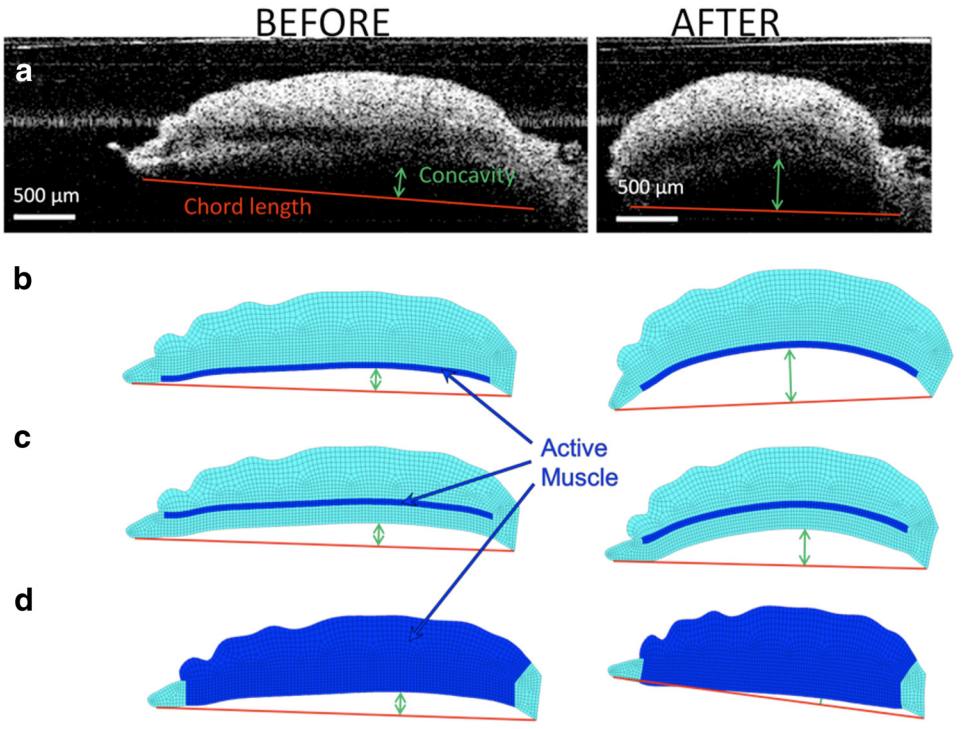

FIGURE 8. Iris chord length and curvature before (*left*) and after (*right*) dilation in (**a**) a typical ex vivo experiment, (**b**) an anatomic realistic model of the iris with the dilator muscle in the posterior, (**c**) an artificial model in which the dilator was positioned anteriorly, and (**d**) an artificial model in which the dilator was thickened throughout the entire iris contour.

DISCUSSION

The major conclusion drawn from this work is that the location of the dilator itself can cause iris anterior bowing. Three different types of experiments (clinical, experimental, and computational) all confirmed the contribution of the dilator's position to a non–pupillary-block–dependent mechanism for anterior bowing.

Although it is possible that the lack of radial symmetry in pinning of the ex vivo iris led to a small artifact, we observed no difference when more pins were used, so the two-pin method was deemed acceptable. We also have found previously[15] that ex vivo irides lose the ability to dilate approximately 5 to 6 hours after death, and it is therefore essential that the eyes be harvested and tested quickly if the iris is the target. It is noted that in vivo studies were on patients who had received LPIs for narrow angles, and some effects that were observed could have been more or less pronounced than they would be in the general population. Healthy subjects are not given LPIs, but LPI is used to treat patients with pigmentary glaucoma, who could provide an alternative test group.

It has been suggested[23] that incompressibility of the iris (or inability of water to escape from the iris stroma) contributes to the risk of angle narrowing or closure. The present study focuses on the contour as described by the posterior surface of the iris, and so no conclusion can be drawn relative to the aforementioned studies, but there may be a synergistic effect between dilator-induced curvature and the pushing of the iris into the angle. Both ideas must also be examined in light of the role of pupillary block.

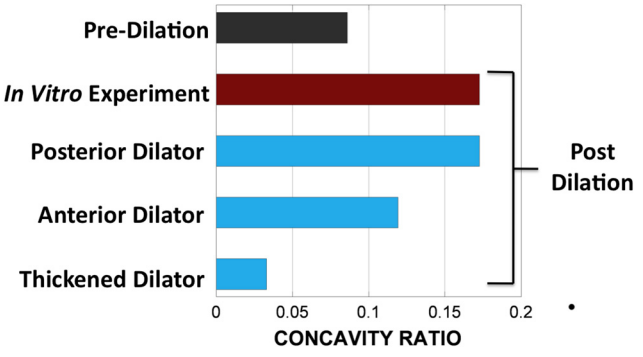

FIGURE 9. Iris concavity ratio before and after dilation in a typical experiment and three models based on the geometry of the experiment. In the realistic model (Fig. 8b), the iris curvature was similar to that of the experiment. Anteriorly positioning (Fig. 8c) or thickening of the dilator muscle (Fig. 8d) in the artificial models led to a predicted curvature inconsistent with the experimental data.

Acknowledgments

The authors thank Heidi Roehrich for help with the histology, and the University of Minnesota Visible Heart Laboratory, the University of Minnesota Experimental Surgical Services, and Lorentz Meats (Cannon Falls, MN) for the provision of porcine eyes.

References

1. Mandell MA, Pavlin CJ, Weisbrod DJ, Simpson ER. Anterior chamber depth in plateau iris syndrome and pupillary block as measured by ultrasound biomicroscopy. *Am J Ophthalmol.* 2003;136:900–903.
2. Nonaka A, Iwawaki T, Kikuchi M, Fujihara M, Nishida A, Kurimoto Y. Quantitative evaluation of iris convexity in primary angle closure. *Am J Ophthalmol.* 2007;143:695–697.
3. Ritch LR. Angle-closure glaucoma: mechanisms and epidemiology. *The Glaucomas*; St. Louis: Mosby; 1996:chap 37.
4. Woo EK, Pavlin CJ, Slomovic A, Taback N, Buys YM. Ultrasound biomicroscopic quantitative analysis of light-dark changes associated with pupillary block. *Am J Ophthalmol.* 1999;127:43–47.
5. Huang EC, Barocas VH. Active iris mechanics and pupillary block: steady-state analysis and comparison with anatomical risk factors. *Ann Biomed Eng.* 2004;32:1276–1285.
6. Yamamoto Y, Uno T, Shisida K, et al. Demonstration of aqueous streaming through a laser iridotomy window against the corneal endothelium. *Arch Ophthalmol.* 2006;124:387–393.

7. He M, Friedman DS, Ge J, et al. Laser peripheral iridotomy in primary angle-closure suspects: biometric and gonioscopic outcomes: The Liwan Eye Study. *Ophthalmology.* 2007;114:494–500.
8. Nonaka A, Kondo T, Kikuchi M, et al. Cataract surgery for residual angle closure after peripheral laser iridotomy. *Ophthalmology.* 2005;112:974–979.
9. Hong C, Park KH, Hyung S-, Song KY, Kim DM, Youn DH. Evaluation of pupillary block component in angle-closure glaucoma. *Jpn J Ophthalmol.* 1996;40:239–245.
10. Prata TS, Palmiero PM, Angelilli A, et al. Iris morphologic changes related to alpha(1)-adrenergic receptor antagonists implications for intraoperative floppy iris syndrome. *Ophthalmology.* 2009; 116:877–881.
11. Santaella RM, Destafeno JJ, Stinnett SS, Proia AD, Chang DF, Kim T. The effect of alpha1-adrenergic receptor antagonist tamsulosin (flomax) on iris dilator smooth muscle anatomy. *Ophthalmology.* 2010;117:1743–1749.
12. Abràmoff MD, Magalhães PJ, Ram SJ. Image processing with ImageJ. *Biophoton Int.* 2004;11:36–42.
13. Liebmann JM, Tello C, Chew SJ, Cohen H, Ritch R. Prevention of blinking alters iris configuration in pigment dispersion syndrome and in normal eyes. *Ophthalmology.* 1995;102:446–455.
14. Amini R, Whitcomb JE, Prata TS, et al. Quantification of iris concavity. *J Ophthalmic Vision Res.* 2010;5:211–212.
15. Whitcomb JE, Barnett VA, Olsen TW, Barocas VH. Ex vivo porcine iris stiffening due to drug stimulation. *Exp Eye Res.* 2009;89:456–461.
16. Al-Qaisi MK, Akkin T. Swept-source polarization-sensitive optical coherence tomography based on polarization-maintaining fiber. *Optics Express.* 2010;18:3392–3403.
17. Yun S, Tearney G, de Boer J, Iftimia N, Bouma B. High-speed optical frequency-domain imaging. *Opt Express.* 2003;11:2953–2963.
18. Hogan MJ, Alvarado JA, Weddell JE. *Histology of the Human Eye: An Atlas and Textbook.* Philadelphia; Saunders; 1971.
19. Whitcomb JE, Amini R, Simha NK, Barocas VH. Anterior-posterior asymmetry in iris mechanics measured by indentation. *Exp Eye Res.* 2011;93:475–481.
20. Heys JJ, Barocas VH, Taravella MJ. Modeling passive mechanical interaction between aqueous humor and iris. *J Biomech Eng.* 2001;123:540–547.
21. Heys J, Barocas VH. Mechanical characterization of the bovine iris. *J Biomech.* 1999;32:999–1003.
22. Amestoy PR, Duff IS, L'Excellent J-Y. Multifrontal parallel distributed symmetric and unsymmetric solvers. *Comput Methods Appl Mech Eng*. 2000;184:501–520.
23. Quigley HA, Silver DM, Friedman DS, et al. Iris cross-sectional area decreases with pupil dilation and its dynamic behavior is a risk factor in angle closure. *J Glaucoma.* 2009;18:173–179.